

Improvement of corrosion resistance of Ti13Nb13Zr alloy using biomedical nanoceramic coatings

Abbas Al-Bawee ^{a*}, Ziad T. Khodair ^a, and Abbas. K. Hussein ^b

^aDepartment of Physics, College of Science, University of Diyala, Baquba, 32002, Diyala Governorate, Iraq

^bDepartment of Material Engineering, Technology University, Baghdad, 10069, Iraq

*Corresponding author. E-mail: abbash77@yahoo.com

Received 29 January 2024, Revised 27 August 2024, Accepted 17 October 2024

ABSTRACT

Metals used for mending fractures or substituting implants due to osteoporosis or injuries need to possess strength, durability, and compatibility with living tissue. For instance, titanium metal exhibits exceptional antibacterial attributes and has brought about enhanced biocompatibility and osseointegration. Titanium-based biominerals may exhibit specific biological functions through their nanoscale coating. The coating process involved electrophoretic deposition and then sintering at 400 °C. The samples were analyzed using XRD, FE-SEM, OCP, and Tafel electrochemical corrosion cell. The treated samples exhibited significantly greater resistance to corrosion compared to their untreated counterparts. The corrosion rate went from 15.13×10^{-5} mmpy for the uncoated sample to 9.564×10^{-6} mmpy for the coated sample by $HA_{70}MgO_{15}YSZ_{15}$ and then to 4.683×10^{-6} mmpy for the coated sample by $HA_{70}MgO_{15}(Al_2O_3)_{15}$ and finally to 2.522×10^{-6} mmpy for the sample coated sample $HA_{55}MgO_{15}YSZ_{15} Al_2O_3_{15}$. The coated samples showed an increase in open circuit potential and a significant decrease in contact angle from 73.848° to 4.513°, indicating improved biocompatibility of medical titanium alloys.

Keywords: Titanium alloy, Nanocomposite coating, Electrochemical corrosion

1. INTRODUCTION

Medical titanium alloys are essential biomedical materials widely used in implants for prosthetics and bone replacement because of their remarkable mechanical strength, low density, corrosion resistance, and biocompatibility [1]. Titanium and its alloys are suitable for use in orthopedic and dental applications due to their excellent biocompatibility. This property ensures that when titanium alloys come into contact with biological tissues, adverse reactions are uncommon. This attribute is crucial for the successful integration and stability of implants within the body [2]. These alloys resist corrosion in physiological conditions by forming a protective oxide layer on their surface. This corrosion resistance ensures the preservation of the structural integrity of implants and prevents the release of harmful metal ions into surrounding tissues [3].

Alloys containing titanium offer desirable mechanical qualities, such as a high strength-to-weight ratio and a low elastic modulus [4]. These characteristics mimic natural bone, allowing improved load transfer from the implant to the surrounding bone while decreasing stress-shielding effects. Ti13Nb13Zr alloys can osseointegrate when implanted into bone, producing a strong, permanent link [5]. This integration not only enhances the stability of the implant but also facilitates effective load transmission and minimizes the likelihood of implant loosening or failure [6].

Bone replacement implants can be made from various Ti13Nb13Zr alloys to meet the needs of each patient [7].

These alloys are sufficiently ductile to undergo casting, forging, machining, or additive manufacturing processes, such as 3D printing, to produce complex designs. Additionally, enhancements to the biological and mechanical properties of the implants can be achieved by applying coatings or treatments to their surfaces [8]. Medical titanium alloys are used in implant prosthetics, including hip, knee, spine, shoulder, and teeth. Patients with degenerative bone disorders, fractures, or joint illnesses can experience improved functionality, reduced discomfort, and an enhanced quality of life as a result of these implants [7]. While medical titanium alloys offer numerous advantages for implants, it is vital to take into account the specific requirements of each patient [8].

These alloys exhibit outstanding mechanical properties and high corrosion resistance, and they are also biocompatible, meaning they do not have adverse effects on the human body when implanted. However, medical professionals, engineers, and material scientists must collaborate to guarantee the most suitable selection and design of bone-replacement prosthetic implants tailored to individual patients [9]. Protected materials have a longer lifespan thanks to the advantages of coatings, which act as a barrier between them and surrounding areas that may damage them, causing environmental deterioration or corrosion of

material in a biological setting is referred to as "bio-corrosion," "biodegradation," or "bio-corrosion" [10, 11]. The term "bio-corrosion" is commonly used to characterize the gradual deterioration of the Ti13Nb13Zr biomedical alloy implanted in the body, which occurs due to its interactions with biological fluids and tissues [12]. The exceptional corrosion resistance of the Ti13Nb13Zr alloy is mainly attributed to the development of a protective oxide layer on its surface. Nonetheless, exposure to harsh conditions or damage to the oxide layer can lead to the onset of bio-corrosion in the implant [13].

Bio-corrosion of the Ti13Nb13Zr biomedical alloy can be influenced by various factors. For instance, the breakdown of the passive oxide layer in certain areas may result in localized corrosion attacks such as pitting or crevice corrosion [14]. Corrosion susceptibility may be heightened in specific regions due to factors such as variations in oxygen levels, pH, or the presence of chloride ions, a phenomenon known as galvanic corrosion. When in electrical contact with the body, dissimilar metals or alloys like the Ti13Nb13Zr alloy and other implant materials can induce galvanic corrosion, accelerating the deterioration of the alloy [15-17].

Biocorrosion is a complex phenomenon that exhibits variability based on an individual's physiological condition. Therefore, collaboration with medical professionals and biomaterials specialists is crucial for assessing the biocorrosion risk and determining optimal strategies for implant selection and monitoring [18]. Electrophoretic deposition (EPD) is an electrochemical method that relies on electrophoresis and deposition. This technique is widely used to create and deposit a variety of materials such as ceramics, metals, polymers, and composites [19]. EPD allows for the creation of uniform and durable coatings or films on conductive surfaces due to its precise management of the deposition process. In the initial procedure [20, 21], particles in a suitable solution are charged by an electric field applied between two electrodes, and they migrate to the electrode with the opposite charge [22]. When particles are allowed to settle at the deposition electrode, a rather consistent and homogenous layer is produced [23-25].

EPD is commonly utilized as a cost-effective and efficient coating technique [26, 27]. Applying calcium phosphate (CaP) to metallic implants can decrease the release of

harmful metal ions and enhance bioactivity, potentially increasing the adoption of EPD [28, 29]. Hydroxyapatite and specific ceramic materials have been extensively employed in biocoating for implant replacement and dental medical applications due to their strong biocompatibility and chemical similarity to natural bone tissue [30, 31]. The main objective of this study is to improve the biocompatibility of titanium replacement implant alloy by improving corrosion resistance and reducing contact angle by using a nanocomposite coating composed of materials with high face compatibility.

2. EXPERIMENTAL WORK

The study employed titanium alloy (Ti13Nb13Zr) for the experiment. Several methods were employed, including the use of energy dispersive X-ray (EDX) to examine the chemical composition of the Ti13Nb13Zr alloy, which is detailed in Table 1. The Ti alloy was segmented using a wire-cut machine operating at a controlled cutting speed and flow rate, specifically planned to minimize heat generation during cutting. According to the required evaluation, the thickness of the samples is determined by their 2 mm and 10 mm radius. One face of the samples was ground utilizing SiC Emerald sheets with grit levels of 220, 400, and 600. They were then cleaned for 15 minutes in an ultrasonic bath of acetone and distilled water. The magnesium oxide nanoparticles (30-55 nm, purity of 99%, white color, 3.140 g/cm³ density) were used to deposit them as coating layers. The hydroxyapatite (30-65 nm, purity of 99%, white color, 4.176 g/cm³ density) was utilized to make the EPD solution. Chitosan, a polymeric material widely utilized in biological applications, serves as a binding agent in nanocomposite materials. Its primary role is to act as an adhesive on the surface of Ti13Nb13Zr alloy. Due to concerns about potential alterations to the nanocomposite phase from heat sources, the electrophoretic deposition method was employed for coating deposition. The EPD technique is straightforward to use. An essential stage in the experimental process for EPD is suspension preparation as shown in Figure 1.

Table 1. Chemical composition of the Ti-13Zr-13Nb alloy, wt.%

Ti	Nb	Zr	O	H	N	Fe	C
Base	12.5	12.5	0.121	0.004	0.01	0.04	0.04

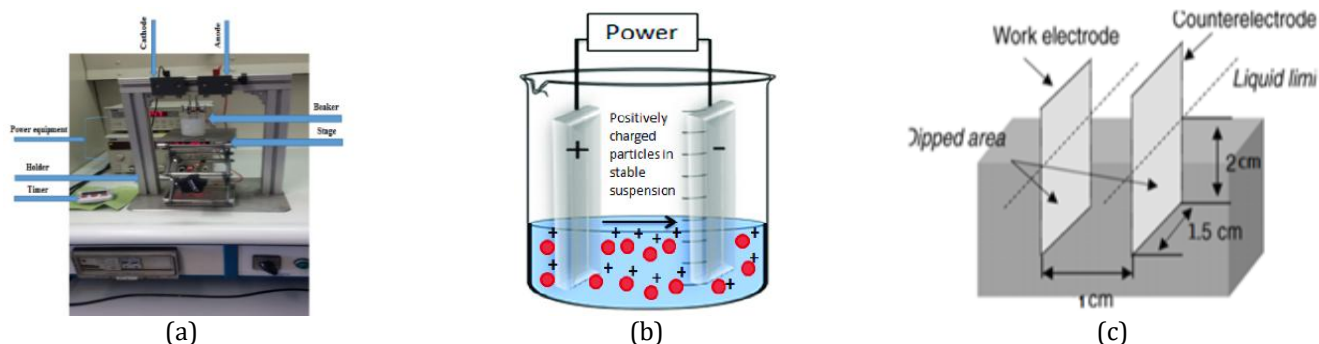


Figure 1. (a) The EPD system and (b and c) diagrammatic representation of the EPD cell configuration

First, 0.5 g/L of chitosan was dissolved in ethanol, with 1% acetic acid as a solvent and 5% distilled water added; subsequently, nanomaterials were added. The suspension was put in a magnetic stirrer for three hours to prevent agglomeration of the nanomaterials, ensuring uniformity in the suspensions. This was followed by sonication using an Ultrasonic Processor (MIXSONIX Incorporated N.Y, USA) for 30 minutes to further de-agglomerate the suspensions. The EPD cell utilized in this study comprises a beaker with two electrodes submerged in the suspension, as illustrated in the system design for EPD employed here. The digital power supply and copper cable were used in the EPD Instruments. The cathode and Anode were made of platinum Ti13Nb13Zr alloy, respectively.

Afterward, the samples' coating was air-dried at room temperature. The electrochemical corrosion circuit generally comprises the following components: Metal Sample - This refers to the material subject to corrosion and can be any metal or alloy vulnerable to corrosion in a corrosive setting. Electrolyte - This conductive medium facilitates the movement of ions between the metal sample and the electrode. It contains simulated body fluid (SBF), Anode and cathode, metallic path, and electrical Load. A corrosion cell is formed when these components are connected, and electrochemical reactions occur. At the Anode, metal atoms are oxidized into metal ions, releasing electrons. These electrons flow through the metallic path to the cathode, where reduction reactions occur. The flow of electrons generates an electric current that can be measured and used to quantify the corrosion rate.

3. RESULTS AND DISCUSSION

3.1. X-ray Diffraction

Figure 2(a) shows the XRD results of the uncoated Ti13Nb13Zr substrate. The base alloy exhibited diffraction patterns corresponding to alpha and beta phases as per JCPDS Card No. 044-1294, with no presence of impurity phases. Upon application of coatings onto the surface alloy, additional peaks emerged due to the introduction of various materials (HA, YSZ, MgO, and Al₂O₃). It also changes the angle of the peaks of each phase of the titanium alloy (beta and alpha), which depends on the effect of the addition. For Figure 2(a), the uncoated substrate, the (002) and (211) alpha titanium phase appeared at the 2θ (38.73°) and (63.47°), respectively. (101) phase of Beta titanium seemed at the 2θ (40°), (102) at the 2θ (53°), and (004) at the 2θ (73°). The (111) zirconium phase appeared at the 2θ (42.5°) and (222) at 2θ (77.23°). (110) Niobium phase appeared at 2θ (35.37°). After the alloy surface was coated with the nanocomposite materials, new phases appeared in addition to the phases mentioned previously. In Figure 2(b), the (211) hydroxyapatite phase appeared in the angle (26.47°), (28.23°) the (101), and (101) phases, respectively, it is seen in two phases of titanium alloy (α-hexagonal and β-centered cubic) structure at different 2θ of 43.582, 50.79°, and 74.67°. Figure 2(c) shows that the peaks of (HA, MgO, and YSZ) are observed following the coating of nanomaterials. The strong presence of these nanocomposite phases is evident from the peaks of HA (211) at 2θ (31.7°), (002) at 2θ (25.8°), (210), (202) and

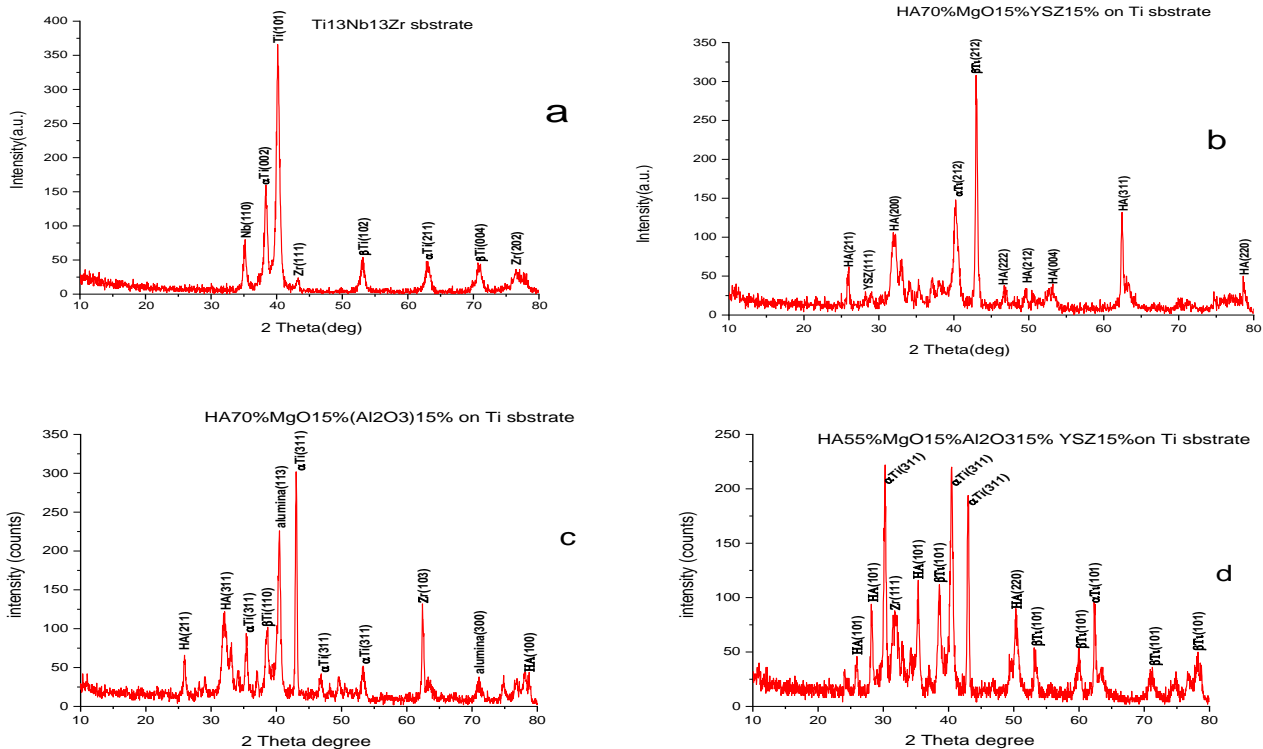


Figure 2. X-ray diffraction examination (a, b, c, d) for different coated and uncoated samples

(422) according to the JCPDS card No. 09-0432. In Figure 2(d), the phase composition of the coating d contains an Al_2O_3 phase at 2θ (47.56°). All figures prove natural formation of $\text{HA}_{70}\text{MgO}_{15}\text{YSZ}_{15}$, $\text{HA}_{70}\text{MgO}_{15}(\text{Al}_2\text{O}_3)_{15}$, $\text{HA}_{55}\text{MgO}_{15}\text{YSZ}_{15}(\text{Al}_2\text{O}_3)_{15}$ coatings on the surface of Ti13Nb13Zr substrates. When examining the uncoated and coated Ti13Nb13Zr, it is observed that the prominent peak lines of the Ti13Nb13Zr phases (111) and (200) decrease in magnitude after undergoing coating with (HA, MgO, YSZ, and Al_2O_3) peaks. This reduction can be attributed to the presence of a nanocoating layer on the titanium alloy surface, which effectively diminishes the visibility of these alloy phases to the extent of their complete disappearance. The XRD patterns of the coated samples showed that the coating layer contains many HA, MgO, YSZ, or Al_2O_3 particles through the appearance of all phases of these nanomaterials that form the nanocoating layer, as evident in these figures. These elements were combined to form a nano-ceramic composite material deposited on the substrate surface. The X-ray diffraction analysis revealed a variety of phases present in the titanium alloy and the ceramic nanomaterials utilized in the surface coating process. In the coated alloy, both the aforementioned phases and new phases characteristic of the ceramic materials used in the coating process were observed. This was also evident in Figure 2(c), where alumina replaced yttria reinforced with zirconia in both the alloy and its coating. Furthermore, Figure 2(d) illustrates the presence of the hydroxyapatite phase alongside all three aforementioned oxides, indicating a uniform composition of the nano-coating material. The distinct presence of all coating materials' phases provides clear evidence of their complete representation.

3.2. Corrosion Behavior Test

The samples were tested for corrosion resistance in a simulated body fluid (SBF), revealing that those coated with the nanocomposite were significantly less susceptible to rust. However, the results of the corrosion examination varied depending on the type of nanocomposite used. For the uncoated substrate, the corrosion rate was measured at 15.13×10^{-5} mmpy. On the other hand, the coated substrate with $\text{HA}_{70}\text{MgO}_{15}\text{YSZ}_{15}$, showed an improved corrosion rate of 9.564×10^{-6} mmpy. The coated sample with $\text{HA}_{70}\text{MgO}_{15}(\text{Al}_2\text{O}_3)_{15}$ displayed a corrosion rate of 4.683×10^{-6} mmpy, and a titanium alloy specimen coated with $\text{HA}_{55}\text{MgO}_{15}\text{YSZ}_{15}(\text{Al}_2\text{O}_3)_{15}$ had a corrosion rate of 2.522×10^{-6} mmpy. Overall, all samples displayed better corrosion resistance than the uncoated sample, but the coated sample

with $(\text{HA}_{55}\text{MgO}_{15}\text{YSZ}_{15}(\text{Al}_2\text{O}_3)_{15})$ stood out as particularly effective compared to other coated substrates.

The application of nanoceramic-coated titanium alloy demonstrates enhanced resistance to corrosion and increased nobility, as demonstrated by higher E_{Corr} and lower I_{Corr} values in the electrochemical cell. The enhanced corrosion resistance of the modified titanium alloy makes it more suitable for use as replacement implants in the medical field compared to other alloys. The findings suggest that a nanocomposite has developed a highly effective protective coating on the surface of the specimens, leading to reduced or negligible release of zirconium or niobium ions with higher corrosion resistance. These ions have the potential to promote bacterial aggregation, which can result in serious health conditions in humans. The open circuit potential (OCP) is a critical factor in achieving a balance between the electrolyte and metallic implant. The simulated body fluid (SBF) was submerged in the samples. OCP was monitored for ninety minutes before the steady-state potential was achieved. Figure 4 shows the open circuit potential of the uncovered and covered substrate with $\text{HA}_{70}\text{MgO}_{15}\text{YSZ}_{15}$, $\text{HA}_{70}\text{MgO}_{15}(\text{Al}_2\text{O}_3)_{15}$, $\text{HA}_{55}\text{MgO}_{15}\text{YSZ}_{15}(\text{Al}_2\text{O}_3)_{15}$, respectively. As compared with uncoated Ti substrate OCP = -0.530 V, for the $\text{HA}_{70}\text{MgO}_{15}\text{YSZ}_{15}$, the OCP = -0.491 V, while the $\text{HA}_{70}\text{MgO}_{15}(\text{Al}_2\text{O}_3)_{15}$, the OCP = -0.449 V and $\text{HA}_{55}\text{MgO}_{15}\text{YSZ}_{15}(\text{Al}_2\text{O}_3)_{15}$, the OCP = -0.346 V. The coated titanium substrates open circuit potential shifted significantly to the noble direction (less negative), indicating increased thermodynamic stability [11, 31-33]. The results in Figures 3 to 4 and Table 2 show the corrosion for the coated and base samples.

3.3. Contact Angle Measurements

The contact angle measurements of both uncoated and coated substrates were obtained when a water droplet was placed on the surface of the sample. The uncoated substrate demonstrated a contact angle of 73.848° . In contrast, the coated samples demonstrated a notable reduction in contact angle. More specifically, the contact angle for sample (b) coated with $(\text{HA}_{70}\text{MgO}_{15}\text{YSZ}_{15})$ ($\text{HA}_{70}\text{MgO}_{15}(\text{Al}_2\text{O}_3)_{15}$), and $(\text{HA}_{55}\text{MgO}_{15}\text{YSZ}_{15}(\text{Al}_2\text{O}_3)_{15})$ were 9.783° , 7.542° , and 4.513° , respectively. The results indicate that the nanocomposite coating exhibits growing compatibility with the human body. Figure 5 and Table 3 present the contact angle values for uncoated and coated Ti13Nb13Zr substrates, as well as for different coatings on Ti13Nb13Zr substrates.

Table 2. The corrosion results for the uncoated and coated specimens

Item	E_{corr} (V)	I_{corr} (A)	Corr. Rate (mmpy)	β_c	β_a	OCP (V)
Substrate	-0.481	1.320×10^{-7}	15.13×10^{-5}	0.211	0.207	-0.530
$\text{HA}_{70}\text{MgO}_{15}\text{YSZ}_{15}$	-0.515	8.342×10^{-8}	9.564×10^{-6}	0.203	0.206	-0.491
$\text{HA}_{70}\text{MgO}_{15}(\text{Al}_2\text{O}_3)_{15}$	-0.482	4.085×10^{-8}	4.683×10^{-6}	0.207	0.206	-0.449
$\text{HA}_{55}\text{MgO}_{15}\text{YSZ}_{15}(\text{Al}_2\text{O}_3)_{15}$	-0.490	2.200×10^{-8}	2.522×10^{-6}	0.207	0.201	-0.346

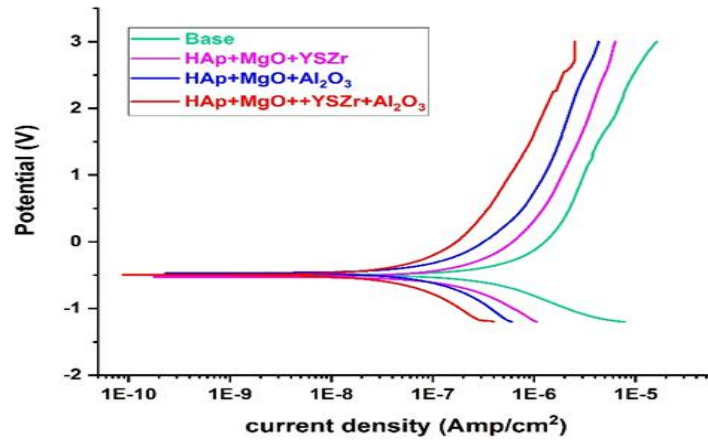


Figure 3. Potentiodynamic polarization curves of coated and uncoated Ti13Nb13Zr samples in simulated body fluid (SBF)

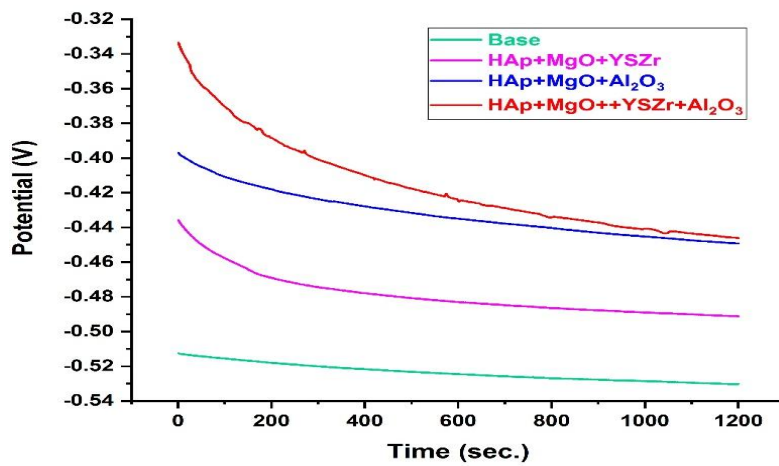


Figure 4. Cumulative concentrations of ions released from exposure in simulated body fluid (SBF)

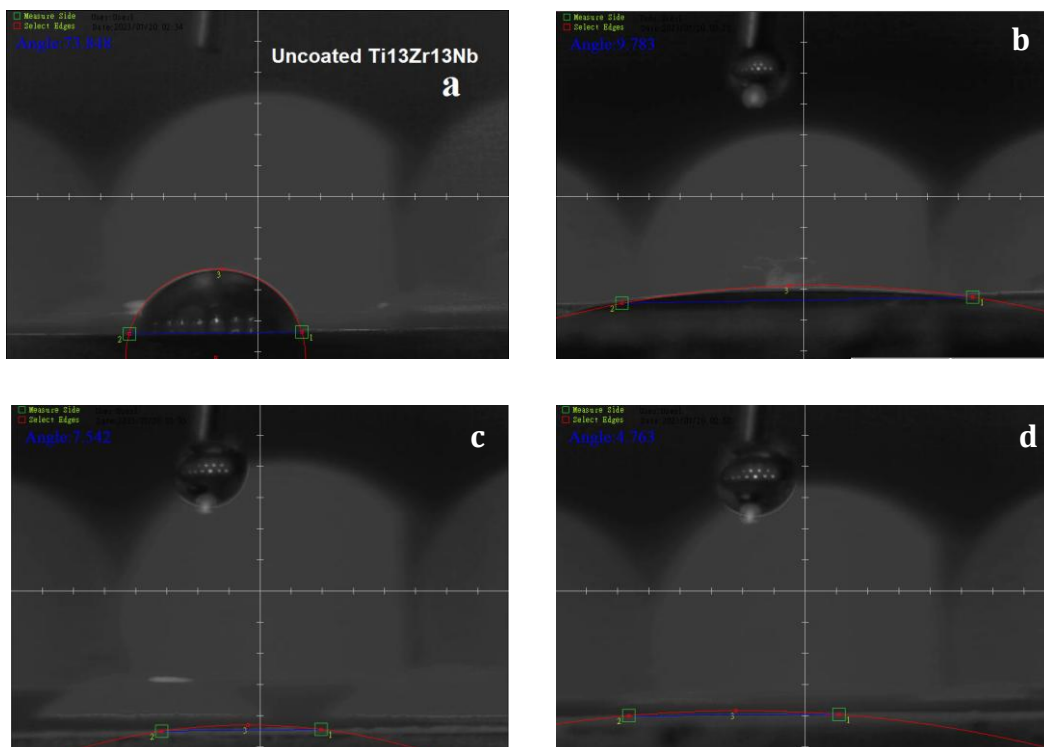


Figure 5. Water contact angle measurements of (a) uncoated and (b, c, d) coated titanium samples.

Table 3. The values of the contact angle of uncoated and coated samples

Item	Contact Angle (°)
Base substrate	73.848
HA ₇₀ MgO ₁₅ YSZ ₁₅	9.783
HA ₇₀ MgO ₁₅ (Al ₂ O ₃) ₁₅	7.542
HA ₅₅ MgO ₁₅ YSZ ₁₅ (Al ₂ O ₃) ₁₅	4.513

3.4. FE-SEM Examination

FE-SEM images for the surface morphology of Ti13Nb13Zr substrates coated with nanocomposite powders at numerous magnifications are shown in Figure 6.

Figure 6(a) demonstrates that substituting YSZ with Al₂O₃ on the coating surface (HA₇₀MgO₁₅YSZ₁₅) led to a reduction in the number of microcracks. Moreover, when (YSZ+Al₂O₃) were combined on the alloy surface to form (HA₅₅MgO₁₅YSZ₁₅(Al₂O₃)₁₅), the nanolayer coating became more uniform and homogeneous, resulting in significantly fewer cracks compared to the previous coated samples. This enhancement contributed to an increase in corrosion resistance.

These cracks are attributed to the rapid evaporation of ethanol and quick drying of the coatings, causing thermal stresses due to differences in thermal expansion, which is a significant factor contributing to cracks on the coating surface. When incorporating nanomaterials (Al₂O₃+YSZ) to (HA+MgO), these substances effectively eradicated the occurrence of cracks, as demonstrated in Figure 6(b). The figure illustrates the progressive enhancement of the nano-coating following each addition. It is crucial to note that

these nanomaterials vary in size, and this discrepancy was a critical factor in achieving homogeneity in the nanocomposite coating to prevent crack formation.

The distribution of pores on the surface of the coated samples appears to be relatively uniform, as shown by Figure 6. These figures also demonstrate the nanoscale dimensions of the nanomaterials utilized in the coating procedure. Furthermore, the coated sample with (HA₅₅MgO₁₅YSZ₁₅(Al₂O₃)₁₅) coating was more stable and homogeneous, and this is consistent with the corrosion resistance results. The corrosion resistance of all samples was notably high in comparison to the initial results

3.5. Thickness measurement

The examination of the thickness of the coating layer revealed that the coated sample (a) with the (HA₇₀MgO₁₅YSZ₁₅) coating had a thickness of 67 μm. Sample (b) coated with the (HA₇₀MgO₁₅(Al₂O₃)₁₅) layer measured 57 μm, while the coating layer for sample (c) coated with (HA₅₅MgO₁₅YSZ₁₅(Al₂O₃)₁₅) was 47 μm. Despite the lower thickness of the coating layer for sample (c), its quality was superior, as indicated by a lower corrosion rate compared to other samples, supported by optical microscope images. Furthermore, despite the identical coating process conditions, the coating layer thickness of ((HA₅₅MgO₁₅YSZ₁₅(Al₂O₃)₁₅) was the smallest, yet it proved to be the most effective among the titanium substrates coated.

Collecting these nanomaterials with different nanoscale sizes formed a more homogeneous nano-coating layer. Figure 7 illustrates the coating thickness layer for coated samples.

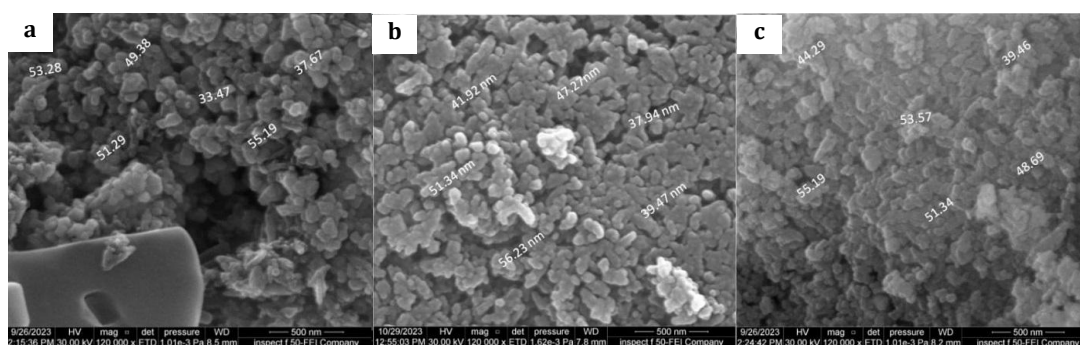


Figure 6. (a, b, c) SEM images. Morphology of surface

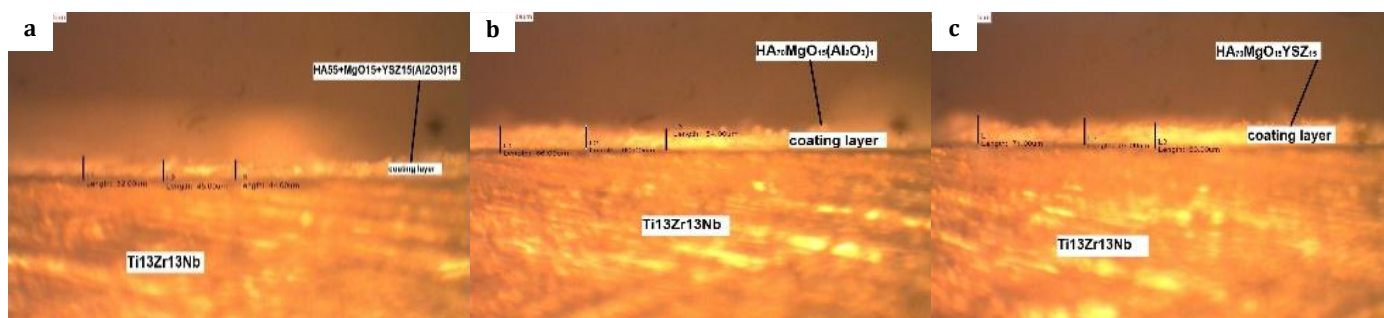


Figure 7. (a, b, c) Thickness of different nanocomposite coating

4. CONCLUSION

The nano-ceramic coating manufactured on the surface of Ti13Nb13Zr alloy showed a significantly lower corrosion rate and thus improved corrosion resistance compared to the uncoated substrate. Among the coated samples, the most effective in terms of corrosion resistance was the one coated with (HA₅₅MgO₁₅YSZ₁₅(Al₂O₃)₁₅). Furthermore, the nano-coating raised the open circuit potential and significantly reduced the contact angle. As a result, the alloy surface becomes hydrophilic, leading to more interconnected tissue growth. This greatly enhances biocompatibility, rendering titanium alloys suitable for biomedical purposes. These results show that the use of these particular nanocomposite materials can enhance the performance and durability of titanium substrates in dental and orthopedic implant applications. Moreover, electrodeposition is an effective method for producing nanolayers for biomedical purposes as it ensures uniform coating molecules, which can be observed through scanning electron microscopy and X-ray diffraction scanning. The combination of hydroxyapatite coating with magnesium oxide is anticipated to bring about substantial improvements in osseointegration and reduce the inflammatory effects of implants as described in the manuscript.

REFERENCES

- [1] X. Han *et al.*, "Surface modification techniques of titanium and titanium alloys for biomedical orthopaedics applications: A review," *Colloids and Surfaces B: Biointerfaces*, vol. 227, p. 113339, Jul. 2023, doi: 10.1016/j.colsurfb.2023.113339.
- [2] Z. Guo *et al.*, "Preparation and characterization of metastable β -type titanium alloys with favorable properties for orthopedic applications," *Journal of Alloys and Compounds*, vol. 949, p. 169839, Jul. 2023, doi: 10.1016/j.jallcom.2023.169839.
- [3] X. Zhang, S. Liu, Y. Liu, H. Guo, and W. Shi, "Titanium Alloy Fabricated by Additive Manufacturing for Medical Applications: Obtaining, Characterization and Application—Review," *Metals*, vol. 13, no. 3, p. 462, Feb. 2023, doi: 10.3390/met13030462.
- [4] V. M. S. Muthaiah, S. Indrakumar, S. Suwas, and K. Chatterjee, "Surface engineering of additively manufactured titanium alloys for enhanced clinical performance of biomedical implants: A review of recent developments," *Bioprinting*, vol. 25, p. e00180, Mar. 2022, doi: 10.1016/j.bprint.2021.e00180.
- [5] X.-Q. Wang, Y.-S. Zhang, and W.-Z. Han, "Design of high strength and wear-resistance β -Ti alloy via oxygen-charging," *Acta Materialia*, vol. 227, p. 117686, Apr. 2022, doi: 10.1016/j.actamat.2022.117686.
- [6] G. Huang, S.-T. Pan, and J.-X. Qiu, "The osteogenic effects of porous Tantalum and Titanium alloy scaffolds with different unit cell structure," *Colloids and Surfaces B: Biointerfaces*, vol. 210, p. 112229, Feb. 2022, doi: 10.1016/j.colsurfb.2021.112229.
- [7] G. Senopati, R. A. Rahman Rashid, I. Kartika, and S. Palanisamy, "Recent Development of Low-Cost β -Ti Alloys for Biomedical Applications: A Review," *Metals*, vol. 13, no. 2, p. 194, Jan. 2023, doi: 10.3390/met13020194.
- [8] J. Ballor, T. Li, F. Prima, C. J. Boehlert, and A. Devaraj, "A review of the metastable omega phase in beta titanium alloys: the phase transformation mechanisms and its effect on mechanical properties," *International Materials Reviews*, vol. 68, no. 1, pp. 26–45, Jan. 2023, doi: 10.1080/09506608.2022.2036401.
- [9] C. Gao *et al.*, "Innovative Materials Science via Machine Learning," *Advanced Functional Materials*, vol. 32, no. 1, Jan. 2022, doi: 10.1002/adfm.202108044.
- [10] M. S. Alias *et al.*, "Encouragement of Graphite and Graphene Oxide Particles on Corrosion Protection Properties for Polyurethane Palm Oil Based UV Curable Coating," *International Journal of Nanoelectronics and Materials (IJNeaM)*, vol. 16, no. Dec, pp. 253–266, Dec. 2023, doi: 10.58915/ijneam.v16iDECEMBER.408.
- [11] N. Contuzzi *et al.*, "Metals Biotribology and Oral Microbiota Biocorrosion Mechanisms," *Journal of Functional Biomaterials*, vol. 14, no. 1, p. 14, Dec. 2022, doi: 10.3390/jfb14010014.
- [12] N. Bruchiel-Spanier, S. Betsis, G. Naim, and D. Mandler, "Electrochemical and electrophoretic coatings of medical implants by nanomaterials," *Journal of Solid State Electrochemistry*, vol. 26, no. 9, pp. 1871–1896, Sep. 2022, doi: 10.1007/s10008-022-05235-6.
- [13] M. Mehdizade, A. R. Eivani, O. Esmailzadeh, and F. Tabatabaei, "Fabrication of osteogenesis induced WE43 Mg-Hydroxyapatite composites with low biodegradability and increased biocompatibility for orthopedic implant applications," *Journal of Materials Research and Technology*, vol. 25, pp. 4277–4298, Jul. 2023, doi: 10.1016/j.jmrt.2023.06.237.
- [14] M. Khethier Abbass, A. N. Jasim, M. Jasim, K. S. Khashan, and M. J. Issa, "Improving Bio Corrosion Resistance of the Single Layer of Nano Hydroxyapatite and Nano YSZ Coating on the Ti6Al4V Alloy Using Electrophoretic Deposition," *Solid State Technology*, vol. 63, no. 6, pp. 18584–18597, 2020.
- [15] J. W. Oldfield and W. H. Sutton, "Crevice Corrosion of Stainless Steels: II. Experimental studies," *British Corrosion Journal*, vol. 13, no. 3, pp. 104–111, Jan. 1978, doi: 10.1179/000705978798276258.
- [16] P. Shetty, S. B. Arya, and V. S. Kodialbail, "Biocorrosion Behavior of Epoxy-Based Multilayer Nanocomposite Coatings," *Journal of Bio- and Tribo-Corrosion*, vol. 9, no. 3, p. 45, Sep. 2023, doi: 10.1007/s40735-023-00763-8.
- [17] N. P. Msweli, "Bio-corrosion response of spark plasma sintered zirconia reinforced titanium in oral environment," Master of engineering (M.Eng) thesis, Faculty of Engineering and the Built Environment, University of Johannesburg, South Africa, 2022.
- [18] D. Prando *et al.*, "Corrosion of Titanium: Part 1: Aggressive Environments and Main Forms of Degradation," *Journal of Applied Biomaterials &*

- Functional Materials*, vol. 15, no. 4, pp. e291–e302, Jan. 2017, doi: 10.5301/jabfm.5000387.
- [19] L. Besra And M. Liu, “A review on fundamentals and applications of electrophoretic deposition (EPD),” *Progress in Materials Science*, vol. 52, no. 1, pp. 1–61, Jan. 2007, doi: 10.1016/j.pmatsci.2006.07.001.
- [20] X. Li, X. Liu, J. Huang, Y. Fan, and F. Cui, “Biomedical investigation of CNT based coatings,” *Surface and Coatings Technology*, vol. 206, no. 4, pp. 759–766, Nov. 2011, doi: 10.1016/j.surfcoat.2011.02.063.
- [21] I. Corni, M. P. Ryan, and A. R. Boccaccini, “Electrophoretic deposition: From traditional ceramics to nanotechnology,” *Journal of the European Ceramic Society*, vol. 28, no. 7, pp. 1353–1367, Jan. 2008, doi: 10.1016/j.jeurceramsoc.2007.12.011.
- [22] S. Kuche Loghmani, M. Farrokhi-Rad, and T. Shahrabi, “Effect of polyethylene glycol on the electrophoretic deposition of hydroxyapatite nanoparticles in isopropanol,” *Ceramics International*, vol. 39, no. 6, pp. 7043–7051, Aug. 2013, doi: 10.1016/j.ceramint.2013.02.043.
- [23] Y. Fukada, N. Nagarajan, W. Mekky, Y. Bao, H.-S. Kim, and P. S. Nicholson, “Electrophoretic deposition—mechanisms, myths and materials,” *Journal of Materials Science*, vol. 39, no. 3, pp. 787–801, Feb. 2004, doi: 10.1023/B:JMSC.0000012906.70457.df.
- [24] Y. E. Feriyanto, Z. S. Putra, N. Ariningtyas, and S. Sitohang, “Bio-corrosion Phenomenon of Titanium Grade 2 Tubes in Condenser of a Steam Power Plant,” *Devotion : Journal of Research and Community Service*, vol. 4, no. 7, pp. 1432–1440, Jul. 2023, doi: 10.59188/devotion.v4i7.524.
- [25] M. Jasim, M. K. Abbass, K. Salah, and A. N. Jasim, “Characterization of electrophoretic deposition parameters of nano hydroxyapatite coating on the Ti6Al4V alloy using DC current,” *AIP Conference Proceedings*, vol. 2213, no. 1, p. 020203, Mar. 2020, doi: 10.1063/5.0000248.
- [26] C. Combes and C. Rey, “Amorphous calcium phosphates: Synthesis, properties and uses in biomaterials,” *Acta Biomaterialia*, vol. 6, no. 9, pp. 3362–3378, Sep. 2010, doi: 10.1016/j.actbio.2010.02.017.
- [27] L. Sorkhi, M. Farrokhi-Rad, and T. Shahrabi, “Electrophoretic Deposition of Hydroxyapatite–Chitosan–Titania on Stainless Steel 316 L,” *Surfaces*, vol. 2, no. 3, pp. 458–467, Jul. 2019, doi: 10.3390/surfaces2030034.
- [28] S. Virtanen, I. Milošev, E. Gomez-Barrena, R. Trebše, J. Salo, and Y. T. Konttinen, “Special modes of corrosion under physiological and simulated physiological conditions,” *Acta Biomaterialia*, vol. 4, no. 3, pp. 468–476, May 2008, doi: 10.1016/j.actbio.2007.12.003.
- [29] M. Hussein, M. Kumar, R. Drew, and N. Al-Aqeeli, “Electrochemical Corrosion and In Vitro Bioactivity of Nano-Grained Biomedical Ti-20Nb-13Zr Alloy in a Simulated Body Fluid,” *Materials*, vol. 11, no. 1, p. 26, Dec. 2017, doi: 10.3390/ma11010026.
- [30] P. C. Rath, L. Besra, B. P. Singh, and S. Bhattacharjee, “Titania/hydroxyapatite bi-layer coating on Ti metal by electrophoretic deposition: Characterization and corrosion studies,” *Ceramics International*, vol. 38, no. 4, pp. 3209–3216, May 2012, doi: 10.1016/j.ceramint.2011.12.026.
- [31] M. Sankar, S. Suwas, S. Balasubramanian, and G. Manivasagam, “Comparison of electrochemical behavior of hydroxyapatite coated onto WE43 Mg alloy by electrophoretic and pulsed laser deposition,” *Surface and Coatings Technology*, vol. 309, pp. 840–848, Jan. 2017, doi: 10.1016/j.surfcoat.2016.10.077.
- [32] A. V. Tibau, B. D. Grube, B. J. Velez, V. M. Vega, and J. Mutter, “Titanium exposure and human health,” *Oral Science International*, vol. 16, no. 1, pp. 15–24, Apr. 2019, doi: 10.1002/osi2.1001.
- [33] B. Łosiewicz *et al.*, “Production and Characterization of the Third-Generation Oxide Nanotubes on Ti-13Zr-13Nb Alloy,” *Materials*, vol. 15, no. 6, p. 2321, Mar. 2022, doi: 10.3390/ma15062321.